Materials and Design 181 (2019) 107930

Contents lists available at ScienceDirect

Materials and Design

journal homepage: www.elsevier.com/locate/matdes

An experimental-numerical study of the adhesive static and dynamic friction of micro-patterned soft polymer surfaces

Alice Berardo [a,1], Gianluca Costagliola [b], Simone Ghio [a,c], Maurizio Boscardin [c], Federico Bosia [b], Nicola M. Pugno [a,d,e,*]

[a] Laboratory of Bio-Inspired & Graphene Nanomechanics, Department of Civil, Environmental and Mechanical Engineering, Università di Trento, via Mesiano, 77, I-38123 Trento, Italy
[b] Department of Physics and "Nanostructured Interfaces and Surfaces" Inter-Departmental Centre, Università di Torino, Via P. Giuria 1, 10125 Torino, Italy
[c] Centre for Materials and Microsystems, Fondazione Bruno Kessler, Via Sommarive 18, I-38123 Povo (Trento), Italy
[d] School of Engineering and Materials Science, Queen Mary University of London, Mile End Road, London E1 4NS, UK
[e] Fondazione E. Amaldi, Ket Lab, Via del Politecnico snc, 00133 Rome, Italy

HIGHLIGHTS

- The effect of patterning on static/dynamic friction of soft polymer surfaces is investigated experimentally and numerically
- Micro-patterns modify macroscopic static friction coefficients between -57 and +20% and dynamic ones between -35 and 30%
- Calculations using an in-house developed 2D Spring-Block model are in good agreement with experimental results

GRAPHICAL ABSTRACT

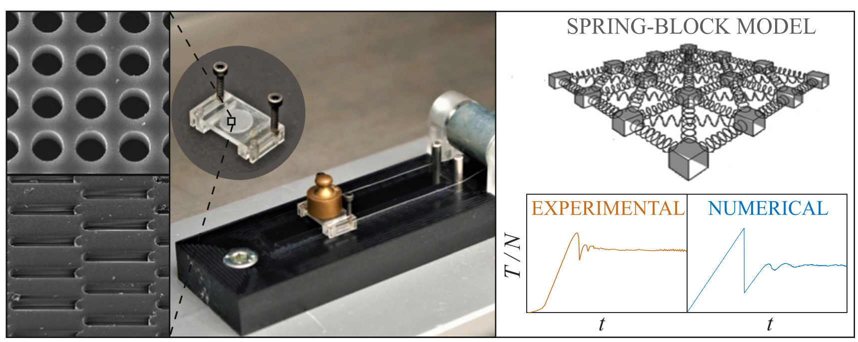

ARTICLE INFO

Article history:
Received 10 May 2019
Received in revised form 9 June 2019
Accepted 10 June 2019
Available online 11 June 2019

Keywords:
Friction
Adhesion
Micro-fabrication
Spring-block model

Data availability:
The raw/processed data required to reproduce these findings cannot be shared at this time due to technical or time limitations.

ABSTRACT

New possibilities have emerged in recent years, with the development of high-precision fabrication techniques, to exploit microscale surface patterning to modify tribological properties of polymeric materials. However, the effect of surface topography, together with material mechanical parameters, needs to be fully understood to allow the design of surfaces with the desired characteristics. In this paper, we experimentally assess the effect of various types of micropatterned Polydimethylsiloxane surfaces, including anisotropic ones, on macroscopic substrate friction properties. We find that it is possible, through surface patterning, to modify both static and dynamic friction coefficients of the surfaces, demonstrating the possibility of achieving tunability. Additionally, we compare experimental observations with the numerical predictions of a 2D Spring-Block model, deriving the material parameters from tests on the corresponding flat surfaces. We find a good quantitative agreement between calculated and measured trends for various micropattern geometries, demonstrating that the proposed numerical approach can reliably describe patterned surfaces when appropriate material parameters are used. The presented results can further contribute to the description and understanding of the frictional effects of surface patterning, with the aim of achieving surfaces with extreme tunability of tribological properties.

* Corresponding author at: Laboratory of Bio-Inspired & Graphene Nanomechanics, Department of Civil, Environmental and Mechanical Engineering, Università di Trento, via Mesiano, 77, I-38123 Trento, Italy.
E-mail address: nicola.pugno@unitn.it (N.M. Pugno).
[1] Present address: C3A - Center Agriculture Food Environment, University of Trento/Fondazione Edmund Mach, Via Edmund Mach, 1 - 38010 San Michele all'Adige (TN), Italy.

https://doi.org/10.1016/j.matdes.2019.107930

1. Introduction

Many practical and industrial applications require the controlled modification of the tribological properties of common manufacturing materials, such as polymers. One approach has been to explore the possibility of modifying the macroscopic friction properties of these materials exploiting specific microscopic surface structures, both in dry and lubricated conditions, instead of applying surface treatments or modifying the material chemistry. Recent experimental results relative to the frictional behaviour of sliding patterned surfaces have been obtained for non-trivial geometric features, e.g. microstructures like grooves, dimples, pillars or honeycomb patterns [1–7]. Surface patterning has been studied for a number of years, and allows accentuating hydrophilic or hydrophobic properties [8–13] or adhesive properties [14–16]. Thus, the effect of surface patterning on the frictional properties of surfaces is of particular interest, including for those applications where control of water-repellent or adhesive behaviour is also required.

Friction between nominally flat surfaces at macroscale is the result of interactions at different length scales spanning from nano- to macro-scale [17–19]. In the case of micropatterned surfaces, the characteristic lengths of the structures also come into play, so that it is difficult to separate the contributions of surface roughness, heterogeneity and patterning, and to identify the dominant mechanisms determining the emergent frictional behaviour. Thus, theoretical and numerical modelling must be adopted in conjunction with experimental observations to explain the effects induced by surface textures and to predict the most suitable configurations for specific purposes.

Models addressing the effect of surface patterning on macroscopic frictional behaviour have been developed for specific cases with the aim of reproducing experimental results [5,20,21]. Another option consists in developing a general simplified model, including the relevant features at the mesoscale and taking into account the microscale by means of effective laws [22], e.g. the Frenkel-Kontorova model [23–25] that can describe the emergent transition to superlubricity due to incommensurate lattice lengths of two sliding layers [26–31]. Another example is the so-called Spring-Block model [32–34], which has been implemented in 1D and 2D to investigate how frictional properties can be modified by hierarchical or complex surface textures [35,36]. In particular, it was shown that the model could provide useful insights on the transition between static and dynamic friction in the presence of structures that modify the surface stress distribution at the onset of sliding. Thanks to its simplicity, the model can provide a clear qualitative understanding of the effects taking place, but due to the adopted approximations, its reliability for precise quantitative predictions remains to be evaluated. In [36], trends consistent with those found in experiments for surface structures were obtained, suggesting that some effects are quite general and may depend on parameters such as shape and size of the surface textures rather than on specific material properties. In this work, one of our aims is to verify to what extent this is true, i.e. to assess the level of reliability of the 2D Spring-Block model [36] in describing frictional properties of structured surfaces.

To physically realize various surface patterns, several techniques have been developed and optimized in the past, including laser surface texturing [37–39], which can provide high precision and speed of manufacturing, especially for applications involving metallic surfaces. On the other hand, micromoulding techniques are a simple and effective alternative to the high costs of laser texturing [3,40,41]. These consist in casting an elastomer using a mould formed by a lithographic technique, and thus transferring the pattern on the elastomer substrate. In the present work, we adopt this method to realize microscale surface texturing on Polydemethilsiloxane (PDMS) substrates in different shapes and sizes, including anisotropic patterns. Variable contact area fractions are considered to account for a wide range of potential applications. Friction tests are then performed on the patterned elastomer substrates against a flat polycarbonate surface and results are compared to the calculations of a 2D version of the Spring-Block model [36], evaluating for the first time the limits of its predictions, with the aim of providing a tool for the precise tribological design of microscopic surface texture.

2. Experimental procedure

2.1. Surface manufacturing

Surface samples are manufactured using PDMS and are realized by direct copy of a patterned silicon substrate. PDMS is widely used in applications where a precise reproduction of a surface design is required (e.g. in microfluidics and in vitro biology applications). The adopted material (Sylgard184) is supplied in two components: a cross-linking curing agent and a pre-polymer base. Polymerization begins when the two liquids are mixed together. The PDMS is first degassed for 30 min directly after mixing and a second time 30 min after deposition on the silicon substrate. The silicon substrate is processed in a Metal-Oxide-Semiconductor pilot line, involving soft-lithography and dry etching to realize micrometric surface structures. Before PDMS moulding, the silicon substrate is coated with a silane Self-Assembly Monolayer to avoid sticking and to promote detachment after curing. Samples are cured at a temperature of 70 °C for 50 min and PDMS samples are peeled from the silicon substrate after cooling.

The chosen surface patterns are periodic arrangements of micro-cavities, as shown in Fig. 1. In particular, three patterns are considered, each characterized by different cavity diameter Φ, pitch distance between cavities p and corresponding contact Area Fraction (*AF*) values, defined as the ratio between the nominal contact area of the patterned sample and the nominal contact area of the flat sample (F). The parameters of the geometries, chosen for their simplicity of fabrication in potential applications, are reported in Table 1. An additional pattern is considered to study the influence of anisotropy (Fig. 1.5, sample S). This pattern presents elongated cavities 40×200 μm in size, with pitch distance $p_y = 120$ μm in the shorter direction and $p_x = 200$ μm in the longer one. Again, this geometry is chosen for its simplicity, while providing marked anisotropy. The cavities are staggered in the longer direction. Both principal directions (x and y in Fig. 1.6) are considered in friction tests.

2.2. Setup for tribological tests

To obtain both the static and dynamic friction coefficients of the aforementioned surfaces, a custom-built tribometer is used (Fig. 2). It is composed of two main polycarbonate parts. The first component (Fig. 2.2) is formed by a tensile machine and a polished polycarbonate surface, which is the reference sliding surface. The other component is the sample holder and slider (enlargement in Fig. 2.1). Samples are glued on the slider, with the surface to be tested in contact with the polycarbonate base. The slider is pulled by a double Dyneema (nearly inextensible) wire, which is connected to the grip of the tensile machine. A variable mass is placed on the top of the slider to change the normal applied force. The tensile machine records the pulling force acting on the wire and transmitted by a frictionless roller, recording the friction force generated by the sample sliding on the polycarbonate base.

2.3. Tribological test procedure

Samples are first glued to the sample holder. Both the test surface and the polycarbonate base are cleaned with ethanol and dried and a given mass is applied on the slider. The test is then performed at constant pulling speed of 0.2 mm/s, which is of the order of values adopted in previous studies [42–44]. Once the detachment force is reached, corresponding to the first peak in the load-displacement curve, the sample starts sliding at an approximately constant force value. When this value

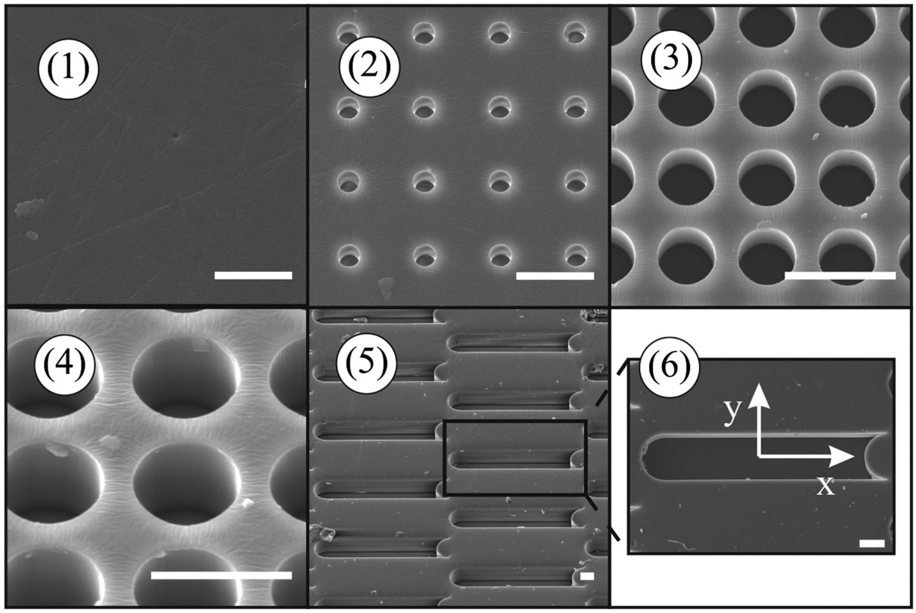

Fig. 1. SEM images showing details of the considered surface patterns: (1) flat surface (sample F). (2) Sample A. (3) Sample B. (4) Sample C. (5) Sample S. (6) Enlargement of a single cavity of sample S. All scale bars are equal to 20 μm.

has stabilized, the test is stopped. The dynamic friction force is taken as the mean value during the sliding phase.

Different masses are used during the friction tests, from 1.5 g (the mass of the sample holder) to about 140 g (with additional weights). Tests are repeated about ten times for each sample and mass (three samples per pattern type) to obtain sufficient statistics. All measurements are carried out at room temperature.

3. Experimental results and discussion

It is known that frictional behaviour of elastomers is a complex phenomenon, usually governed by interfacial properties and dissipation mechanisms (e.g. see [42,45,46]). Adhesion and friction are strictly correlated, and both can depend on sliding velocity, applied normal load and molecular weight, but in the range of small velocities, typically between 0.1 mm/s and 1 mm/s, the dependence of macroscopic friction coefficients on velocity is generally considered negligible [47]. In this study, all tests were performed at the same sliding speed of 0.2 mm/s. Fig. 3 shows the tangential force variation as a function of time for different surface textures. The force is normalized by the static friction force to provide a qualitative comparison on the same scale for each sample. As explained in the previous section, both the static and the dynamic friction forces can be determined from these tests. We report one test for each pattern type, i.e. the friction force normalized by its maximum value obtained in the same test, to highlight behaviour of the different samples. The tests show considerable stick-slip behaviour between the polycarbonate and flat PDMS samples (Fig. 3.1), especially at the beginning of sliding, but this effect becomes less evident for higher applied loads [3,40]. The plots highlight some differences between patterns, especially for sample C (Fig. 3.4), for which static and dynamic friction forces are similar, with limited stick-slip effects.

To better highlight the dependence of the friction force on the pattern type, Fig. 4 shows the results for different applied pressures, both for static and dynamic friction. Since the generalized Coulomb friction law is a good approximation for the macroscopic frictional behaviour of these samples, the experimental results have been fitted using the equation $T = \mu N + \tau_0 A$, where T is the tangential/friction force, μ is the friction coefficient, N is the applied normal load, τ_0 is the adhesive shear strength, and A is the nominal contact area. From the fits, μ and τ_0 are obtained, both for static and dynamic friction (reported in Table 2). Macroscopic friction coefficients decrease non-linearly with increasing applied normal load. For a small or near-zero normal load, results display a large standard deviation, mainly due to difficulties in setting identical initial conditions for all the samples (positioning on the setup was done by hand). Conversely, the standard deviation decreases for increasing normal loads. This also applies to sample C, although some oscillations occur.

Results obtained for sample S highlight the effect of surface pattern anisotropy and sliding along two different directions. Due to the elongated holes, which are longer in the x direction than in the y direction, the friction force is greater when the sample slides along x, especially for small loads. A similar result was found in [40], where the authors studied friction parallel and perpendicular to wrinkled surfaces, observing that for sliding parallel and perpendicular to the wrinkles, the sliding frictional force decreased compared to a flat surface, the greater decrease being for the perpendicular direction.

From experimental results, one can deduce how surface patterns influence the frictional behaviour of the PDMS samples. Sample A is characterized by the smallest cavities and larger spacing, so that its friction coefficients are the closest to those of the flat samples. In comparison, samples B and C display smaller friction forces as a function of the applied normal load. This is partly due to a decrease of the real contact area of the textured samples, as discussed in [3], but also to stress concentrations around surface features and the effect of adhesion, which has a higher relative influence at smaller loads, especially on surfaces with higher texture density.

Table 1
Geometrical characteristics of considered surface patterns. Nominal Area Fraction (*AF*) is calculated as the ratio between the areas of a patterned sample with respect to that of a flat surface (sample F). The pitch distances are also reported (p_x and p_y).

Sample	*Hole diameter* Φ (μm)	*Hole area* (μm^2)	$p_x \times p_y$ (μm^2)	*Nominal AF*
F	–	–	–	1
A	5	$\pi 5^2/4$	20 × 20	0.95
B	10	$\pi 10^2/4$	15 × 15	0.65
C	15	$\pi 15^2/4$	20 × 20	0.56
S	–	40 × 200	220 × 120	0.67

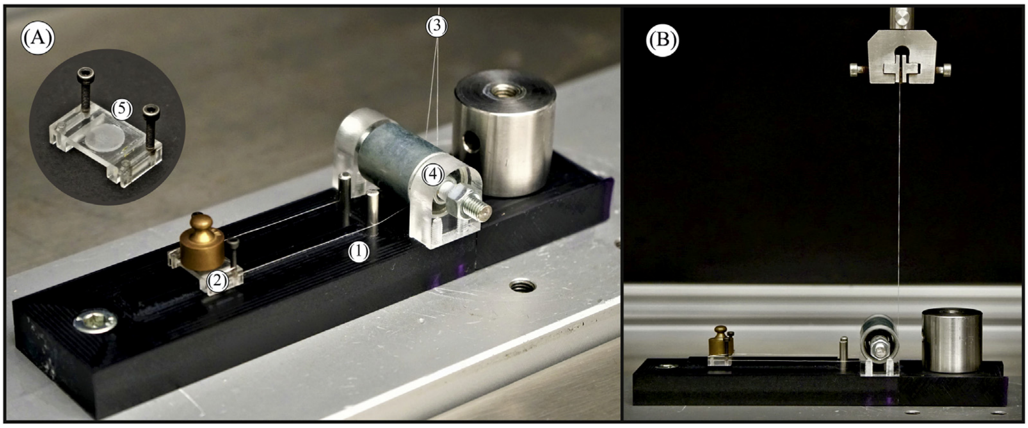

Fig. 2. 1) Details of the custom-built tribometer. A flat polycarbonate surface is fixed to a tensile machine (a). A transparent sample holder (b) can slide on the polycarbonate surface, pulled by two nearly inextensible wires (c), which are connected to the grip of a tensile machine. A frictionless roller (d) transmits the imposed velocity from the machine to the sample holder. Each PDMS surface is attached to the transparent support (e) and loaded with different known weights. 2) Side view of the setup.

4. Numerical simulations

4.1. Model formulation

Sliding friction simulations of the patterned surfaces are performed using the 2D Spring-Block model previously introduced in [36]. In the model, the contact surface is discretized into elements of mass m, each connected by springs to the first eight neighbours and arranged in a regular square lattice with N_x blocks along the x-axis and N_y blocks along the y-axis (Fig. 5.1). The distances between blocks on the two axes are, l_x and l_y, respectively. The equivalence of the spring-mass system with a homogeneous elastic material can be imposed by applying the method illustrated in [47] in the case of plane stress. In this way, the stiffness of the springs parallel to the x- or y-direction in the plane of the material is $K_{int} = 3/4\, E\, l_z$, where E is the Young's modulus and l_z is the thickness of the layer, and the stiffness of the diagonal springs is $K_{int}/2$. This implies that the Poisson's ratio of the modeled homogeneous material is fixed to 1/3 and $l_x = l_y = l$ (the adopted mesh is similar to that used in [34]). The force exerted on the i–th block by the neighbouring j-th block can be written as: $F_{int}^{(ij)} = k_{ij}\,(r_{ij} - l_{ij})(r_i - r_j)\,/\,r_{ij}$, where r_i, r_j are the position vectors of the two blocks, r_{ij} is the modulus of their distance, l_{ij} is the modulus of the rest distance and k_{ij} is the stiffness of the spring connecting them.

All the blocks are connected to the slider through springs of stiffness K_S (Fig. 5.3), which are related to the shear modulus of the material $G = 3/8\, E$, and, by simple calculation, $K_s = K_{int}\,(l\,/\,l_z)^2$. We set for simplicity $l_z = l$. The slider moves at a constant velocity v lying in the xy plane, so that the force exerted by the shear springs on the i-th block at time t is $F_s^{(i)} = (vt + r_i^0 - r_i)$, where r_i^0 is the initial resting position. We define the total driving force as $F_{mot}^{(i)} = F_s^{(i)} + F_{int}^{(ij)}$. Each block is subjected to a normal force $F_n^{(i)} = pl^2$, where p is the applied pressure. A damping force term is added to avoid artificial block oscillations, $F_d^{(i)} = -m\,\gamma\,u_i$, where γ is the damping coefficient, which we fix to $\gamma = 500\ \mathrm{ms}^{-1}$ in the underdamped regime, and u_i is the velocity vector of the i-th block.

The interaction between the blocks and the rigid plane is modeled as in our previous work [36]: each block is subjected to the fundamental

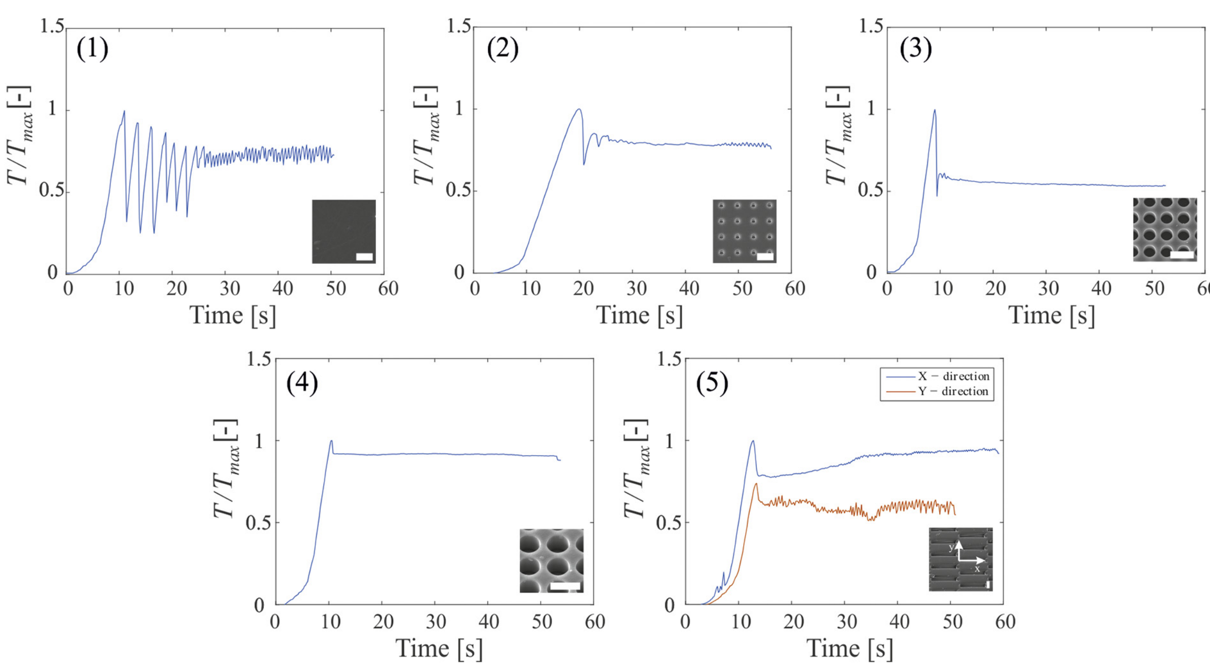

Fig. 3. Examples of friction tests with the described setup; the friction force T is normalized with respect to the peak value of the respective test, which corresponds to the static friction force T_{max}: (1) Flat PDMS surface (sample F). (2) Sample A. (3) Sample B. (4) Sample C. (5) Sample S, along x- and y- directions. All scale bars are equal to 20 μm.

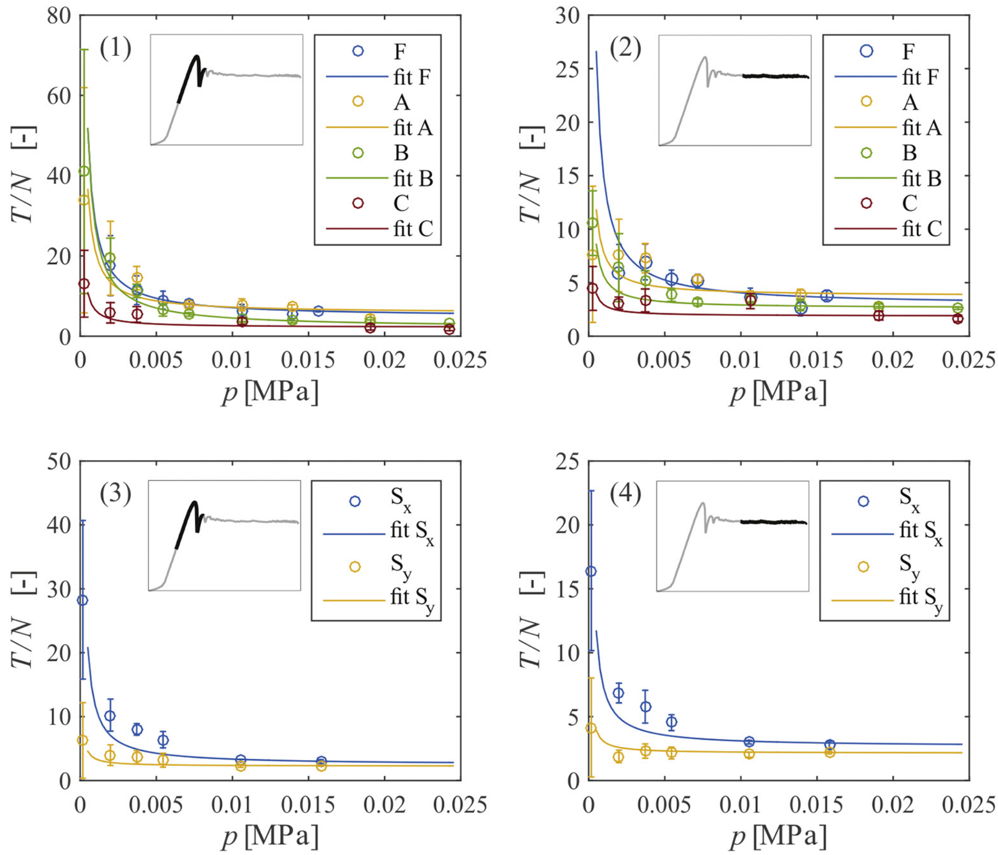

Fig. 4. Experimental apparent friction (T/N) test results. Mean values are reported as dots, while the standard deviation of the mean is shown with error bars. Plots report the ratio between the static or dynamic friction force (T) and the applied normal load (N) as a function of the applied nominal pressure ($p = N/A$, with A the total nominal sample area). The experimental data are fitted by using the generalized Coulomb friction relation $T/N = \mu + \tau_0/p$, where μ is the static or dynamic friction coefficient, while τ_0 is the adhesion force normalized by the nominal area of contact. Fitting parameters μ and τ_0 are reported in Table 2. (1) Static friction coefficients of flat surfaces (samples F) and samples A, B and C. (2) Dynamic friction coefficients of flat surfaces (samples F) and samples A, B and C. (3) Static friction coefficients of samples S, along both x and y directions. (4) Dynamic friction coefficients of samples S, along both x and y directions.

Amontons-Coulomb (AC) friction force with local static and dynamic friction coefficients, respectively $\mu_s^{(i)}$ and $\mu_d^{(i)}$, which are assigned randomly for each block at the beginning of the simulation from a Gaussian statistical distribution $g(\mu_{s,d}^{(i)}) = (2\pi\sigma)^{-1} \exp[-(\mu_{s,d}^{(i)} - (\mu_{s,d})_m)2 / (2\sigma_{s,d}^{\ 2})]$. $(\mu_{s,d})_m$ denotes the mean of the microscopic friction coefficients for the static and dynamic case, respectively, and $\sigma_{s,d}$ is its standard deviation. Thus, the friction force on the i-th block can be described as

Table 2
Linear interpolation ($T/N = \mu + \tau_0/p$) parameters for experimental results and corresponding numerical estimations.

Sample	Experimental results				Numerical estimations			
	μ		τ_0 [kPa]		μ		τ_0 [kPa]	
	Mean	St. dev	Mean	St. dev	Mean	St. dev	Mean	St. dev
Static friction								
F	4.76	0.73	23.45	9.24	4.780	0.013	23.44	0.06
A	5.71	2.36	15.41	20.03	4.150	0.006	17.71	0.04
B	2.05	0.40	24.85	7.46	3.760	0.006	9.83	0.04
C	2.18	1.19	4.30	6.15	4.000	0.032	7.47	0.08
S_x	2.44	1.55	9.17	12.13	3.290	0.006	10.84	0.03
S_y	2.25	0.22	1.16	2.07	3.250	0.006	10.12	0.01
Dynamic friction								
F	2.88	1.39	11.85	11.27	2.879	0.003	11.89	0.01
A	3.75	1.64	4.02	9.47	2.864	0.002	11.17	0.01
B	2.62	0.32	2.98	2.55	3.036	0.008	6.02	0.05
C	1.88	0.78	1.05	2.01	3.107	0.015	4.85	0.08
S_x	2.67	0.87	4.52	5.12	2.866	0.005	8.57	0.01
S_y	2.14	0.16	0.09	0.84	2.851	0.005	8.60	0.03

follows: while the block is at rest, the friction force $F_{fr}^{(i)}$ opposes the total driving force, i.e. $F_{fr}^{(i)} = -F_{mot}^{(i)}$, up to a threshold value $F_{fr}^{(i)} = \mu_s^{(i)} F_n^{(i)}$. When this limit is exceeded, a constant dynamic friction force opposes the motion, whose modulus is $F_{fr}^{(i)} = \mu_d^{(i)} F_n^{(i)}$. Furthermore, since experimental data in this work shows non-negligible adhesion effects in the friction force in the limit of zero pressure, a constant term is added to both static and dynamic friction forces. Thus, the static friction threshold for the i-th block is $F_{fr}^{(i)} = \mu_s^{(i)} F_n^{(i)} + F_{as}$, where F_{as} is the same for all blocks and includes all the possible adhesion effects in the static phase. The dynamic friction force is $F_{fr}^{(i)} = F_{ad} + \mu_d^{(i)} F_n^{(i)}$, where F_{ad} is the adhesion term in the dynamic phase. In the case of patterned surfaces, areas corresponding to cavities are attributed friction coefficients equal to zero.

This model is an approximation of friction/adhesion effects, and other microscopic formulations are possible [19]. However, it is the simplest way to account for adhesion effects without adding specific details of the microscopic structure. Our aim is to test its validity limits comparing it with experimental results.

The motion of a block i is described by Newton's equation:

$$m\, a^{(i)} = \Sigma_j\, F_{int}^{\ (ij)} + F_s^{\ (i)} + F_d^{\ (i)} + F_{fr}^{\ (i)}$$

where $a^{(i)}$ is the block acceleration. The overall system of equations can be solved using a fourth-order Runge-Kutta algorithm to find the model time evolution.

From the equation of motion of all blocks the total tangential friction force can be calculated through the total force exerted by the slider, i.e. $T(t) = \Sigma_i F_s^{(i)}(t)$, which corresponds to that measured in experiments. A

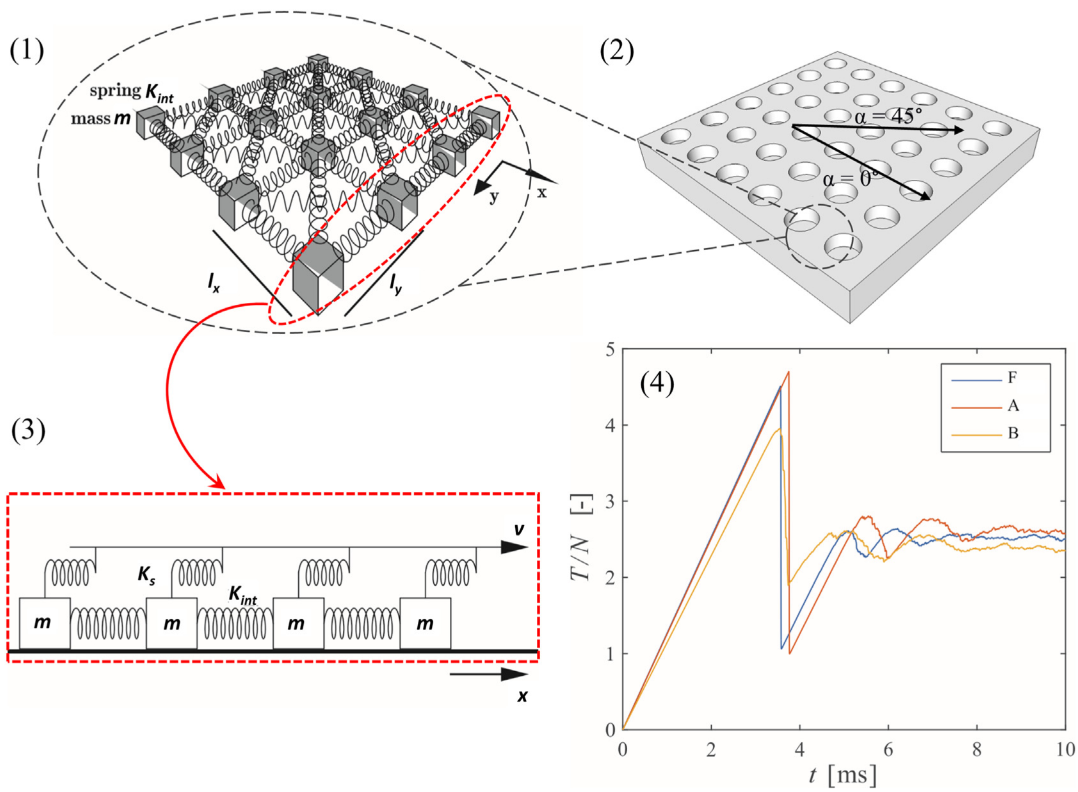

Fig. 5. (1) Schematic of the 2D Spring-Block model with the notation used in the text. Mesh of the internal springs on the surface (shear springs are not shown). (2) Example of a patterned surface, where the main sliding direction is set to $\alpha = 0°$. (3) Side view showing the slider moving at constant velocity v, pulling the sample through shear springs. (4) Typical simulation outputs, showing the time evolution of the friction coefficient for different types of samples.

typical behaviour of T as a function of time is shown in Fig. 5.4. From this curve it is possible to extract the static friction force $T_{max} = max_t\, T(t)$, i.e. the first force peak. To account for statistical effects, the simulations are iterated various times, extracting each time new random local friction coefficients and determining a statistical average of any observable. The integration time step is 10^{-8} s, which is sufficient to reduce integration errors below the statistical uncertainty due to the model iterations [36].

4.2. Model parameters

The numerical model contains a number of parameters that need to be tuned by fitting experimental data, although some degree of approximation is inevitable since experimental conditions cannot be replicated exactly. For example, the Poisson's ratio of the model is constrained to 1/3 due to the requirement of equivalence with a continuous material, while the PDMS real value is closer to 0.5. Since mesh deformations during the simulation are less than 1% of the discretization length, we assume that this approximation is not influential. Although the square mesh is not isotropic, we have verified that for a non-patterned surface, results of macroscopic friction coefficients do not depend on the sliding angle. Moreover, averaging over random orientations is required to account for the uncertainty on the experimental sliding angle (as explained below).

The slider velocity, the applied pressure, the material density and Young's modulus are taken from experimental values. Thus, the mass of the block is $m = \rho\, l^3$, with $\rho = 1.012$ g/cm^3. The Young's modulus is $E = 0.8$ MPa [46], and the applied pressure varies between 3 kPa and 25 kPa. The modulus of the slider velocity is $v = 0.2$ mm/s. In order to reduce the computational times, simulation time scales have been reduced with respect to those used in the experiments (see Fig. 5.4) by adjusting the arbitrary parameter l_z. However, we have verified that modifications on friction coefficients due to a reduced time scale are smaller than the statistical uncertainty on model results. The sliding direction with respect to the (x,y) orientation is randomly chosen at each simulation at an angle α, to account for the uncertainty in the sliding direction in experiments. Thus, the velocity vector of the slider is $\mathrm{v} = (\mathrm{v}\cos(\alpha), \mathrm{v}\sin(\alpha))$. For flat and patterned samples A, B, C the angle is chosen with a uniform distribution in the range [0°, 90°], which is sufficient to emulate the experimental setup due to the symmetry of the samples. For anisotropic samples S, which are designed with a precise sliding direction ($\alpha = 0$ for S along the x-axis and $\alpha = 90°$ for sliding along the y-axis), the uncertainty is reduced and the angle is chosen within a range [−10°, 10°] around the nominal sliding angle.

The local friction coefficients and adhesion force of the model are obtained by fitting the experimental data for a flat (non-patterned) surface, i.e. we set these local parameters to obtain, in the flat case, the same global friction coefficients and total adhesion found in experiments. The average values and standard deviations are $\mu_s)_m = 5.5$, $\sigma_s = 0.195$ and $\mu_d)_m = 2.9$, $\sigma_d = 0.15$ for the local static and dynamic friction coefficients, respectively. The adhesion terms are $F_{as}/l^2 = 23.45$ kPa and $F_{ad}/l^2 = 11.60$ kPa.

The spring mesh discretization length is fixed to $l = 5$ μm, which corresponds to the smallest feature of the experimental surface structures. The total number of blocks required to match the size of the experimental sample would be very high, but it is not necessary to reproduce the entire specimen. As discussed in [36] the resulting qualitative behaviour is not influenced by the number of blocks and the only effect of discretization is the decrease of the macroscopic static friction coefficients. Since there is already a set of free parameters, e.g. local friction coefficients and the adhesion, which need to be tuned in order to match the macroscopic coefficients with the experimental one, it is equivalent to fix a smaller number of blocks and to consequently tune the other parameters. Thus, the lateral number of blocks is $N_x = N_y = 85$, which allows to simulate all the different samples with the same mesh while adequately modelling the cavity geometries.

We approximate the circular holes by means of squares with sides of the same length as the circle diameter and the same spacings between neighbouring cavities. Although the numerical model does not replicate the exact area and geometry of the holes, simulations using with a finer discretization mesh (i.e. reduced discretization length), which better approximate the circular shape, do not provide substantially different results. The same local friction coefficients of the flat surfaces are adopted for the regions of the patterned samples in contact with the substrate. In order to compare the numerical simulations with the experimental results, data must be normalized with respect to the total normal force $N = \Sigma_i F_n^{(i)}$, so that comparisons are made for T/N, i.e. the macroscopic friction coefficient, as a function of pressure p.

5. Discussion

In Figs. 6 and 7, we show the comparison between experimental and numerical results for static and dynamic friction forces, respectively, as a function of the applied normal load. For both series of data, results are fitted using a linear interpolation (red line for experimental and green for numerical), as $T = A{\cdot}\tau_0 + \mu{\cdot}N$. Results obtained for the linear interpolation are also reported in Table 2.

The parameters of the fitting curve display a dependence on the considered surface structure. Once the input model parameters are tuned using experimental data for a flat surface, the numerical calculations for static friction coefficients appear to be in good agreement with experimental results. The model is able to reproduce the correct range of friction values for the different A, B, C samples and for the anisotropic patterns S_x, S_y. This means that, despite the approximations, the model correctly accounts for the stress concentrations occurring at the edges of these structures and is able to capture the underlying mechanisms of the transition from the static to the dynamic phase in the presence of surface features. A good quantitative description of the behaviour of samples A and S_x is found. These are also the samples with a closer match for τ_0 values, while for other samples the calculated variations are slightly smaller.

This can be explained by considering that the adhesion term found in experiments is actually the sum of various effects not directly included in the model, e.g. deformation of the pattern geometries, variation of the effective contact area during sliding, and possible "suction-cup" effects. Thus, the model is less reliable from the quantitative point of view when these factors become more influential.

Numerical dynamic friction coefficients display smaller variations with respect to the experimental values for all types of patterns, and the calculated macroscopic adhesion term is proportional to the effective contact area. This is only partially true for experimental data. As expected, the current formulation of the model is less accurate in describing this phase of the sliding, probably mainly due to the implicit model assumption that pattern shapes remain unvaried during sliding, which may not be strictly true for a soft material like PDMS.

In Fig. 8, we analyse the results of the fit of Table 2 as a function of the corresponding Area Fraction (*AF*) of the different surface structures. Experimental results are correlated to this parameter by adding the curve $T = T_{flat}{\cdot}AF$ (where T_{flat} is the fitting data for the flat surface) to the plot. Friction coefficients and adhesion terms display a linearly decreasing trend with *AF* for all isotropic patterns and for the anisotropic S_x pattern, i.e. when the larger side is aligned with the sliding direction. Results for the S_y pattern appear as outliers in the fit of τ_0. This confirms that area variations due to PDMS deformation influence the global value of τ_0 in the experimental results for different sliding directions on asymmetric patterns, Except for this, both numerical and experimental results are consistent with a three-term friction law $T = \mu\, N + a\, AF + b$, where a and b are constants, so that the adhesion term corresponds to $\tau_0 = a\, AF + b$ for a fixed area fraction [47,48].

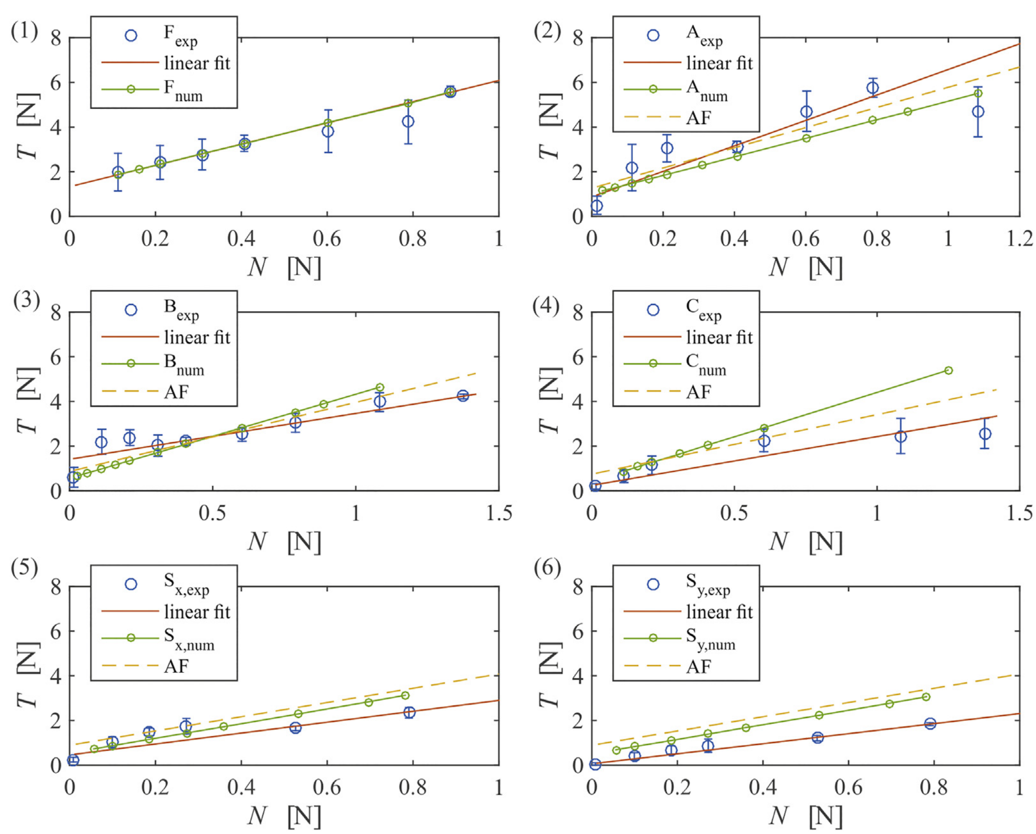

Fig. 6. Static friction force T as a function of the applied normal load (N): experimental data (blue circles), linear fit (red line), numerical simulations (green line), *AF* prediction curve (yellow dotted line). (1) Flat surface (sample F); (2) A sample; (3) B sample; (4) C sample; (5) S sample - sliding along the x direction; (6) S sample - sliding along the y direction. (For interpretation of the references to color in this figure legend, the reader is referred to the web version of this article.)

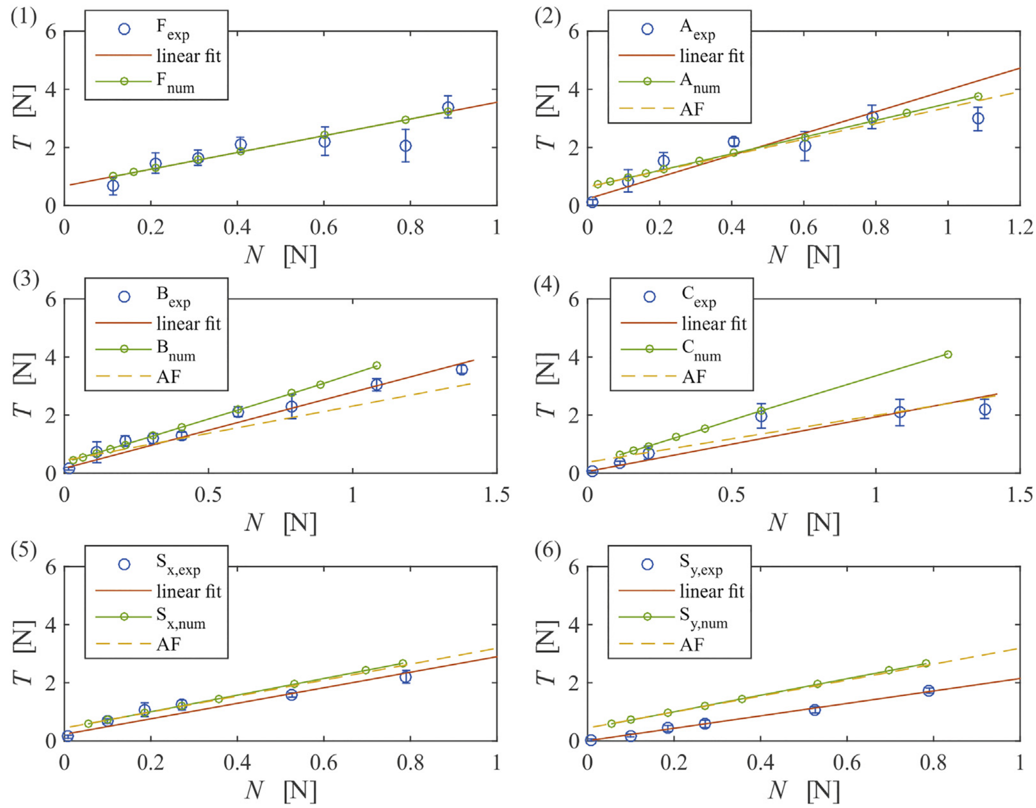

Fig. 7. Dynamic friction force T as a function of the applied normal load (N): experimental data (blue circles), linear fit (red line), numerical simulations (green line), AF prediction curve fit (yellow dotted line). (1) Flat surface (sample F); (2) A sample; (3) B sample; (4) C sample; (5) S sample - sliding along the x direction; (6) S sample - sliding along the y direction. (For interpretation of the references to color in this figure legend, the reader is referred to the web version of this article.)

Overall, results show that the 2D Spring-Block model can be used for a qualitative description of the dynamic friction behaviour, and for a quantitative description of the static friction behaviour of elastic micropatterned surfaces. The necessary tuning of model parameters can be performed once and for all for a given material system and these remain valid for varying surface patterns, at least if the same surface preparation procedure is adopted. The current formulation is reliable for the static phase in a regime of slow sliding, small-intermediate pressures and negligible effects due to pattern deformations during the sliding.

6. Conclusions

In conclusion, we have presented a combined experimental and numerical study on static and dynamic friction of micro-patterned PDMS surfaces on a flat substrate. Experimental results were performed with a custom-made tribometer that allowed the evaluation of friction forces at a constant sliding velocity and for varying normal applied loads. Various types of simple micro-patterns were considered, from equally spaced circular cavities to an array of elongated cavities, to evaluate the role of pattern spacing and anisotropy. Results show good repeatability and

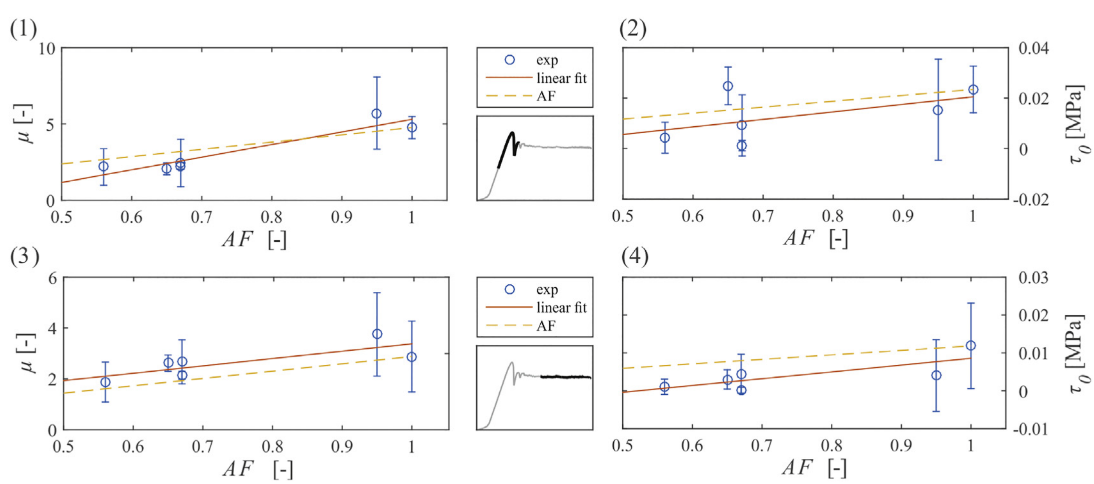

Fig. 8. Experimental and numerical friction coefficient dependence on the area fraction (AF): comparison between μ and τ_0 obtained from the linear fit of the experimental data (the red lines are the fits of these parameters), μ and τ_0 obtained with numerical simulations and the same parameters found assuming $T = T_{flat} \cdot AF$. (1) Static friction coefficient; (2) static adhesion coefficient; (3) dynamic friction coefficient; (4) dynamic adhesion coefficient. Due to approximations in the numerical model, the AF of the samples is slightly different: 0.94 (sample A), 0.57 (sample B), 0.46 (sample C) and 0.72 (sample S_x and S_y). (For interpretation of the references to color in this figure legend, the reader is referred to the web version of this article.)

consistency, with a decrease of macroscopic apparent friction coefficients as a function applied normal load. Anisotropic patterns generate a variation of friction forces of up to 300% depending on the sliding direction in the plane, thus allowing the generation of directionally-tuned friction. Numerical calculations using the 2D Spring-Block model, modified to include adhesion, show considerable agreement with experimental results, correctly reproducing normal load dependence and static friction coefficient absolute values, both for isotropic and anisotropic patterns. Results provide further evidence of the reliability of the presented model in the case of friction of 2D patterned surfaces. This can be of great interest for the calculation of frictional properties of surface patterns, limiting the need for experimental tests, or for the design of novel surface texture designs for applications, which can enable control and tuning of their frictional and adhesive properties.

Abbreviations

PDMS polydemethilsiloxane
AF Area Fraction

Funding sources

EU H2020 Graphene Flagship Core 2 No. 785219 (WP14 "Composites").

EU H2020 FET Proactive "Neurofibres" grant No. 732344.

Italian Ministry of Education, University and Research (MIUR) "Departments of Excellence" grant L.232/2016.

Italian Ministry of Education, University and Research (MIUR) ARS01-01384-PROSCAN Grant.

Italian Ministry of Education, University and Research (MIUR) PRIN-20177TTP3S Grant.

Fondazione San Paolo "Metapp" Grant n. CSTO160004.

CRediT authorship contribution statement

Alice Berardo: Investigation, Methodology, Writing - original draft, Writing - review & editing. **Gianluca Costagliola:** Investigation, Methodology, Writing - original draft, Writing - review & editing. **Simone Ghio:** Investigation, Methodology. **Maurizio Boscardin:** Investigation, Methodology. **Federico Bosia:** Investigation, Methodology, Supervision, Writing - review & editing. **Nicola M. Pugno:** Conceptualization, Resources, Funding acquisition, Investigation, Methodology, Supervision, Writing - review & editing.

Acknowledgments

Computational resources were provided by the C3S centre at the University of Torino (c3s.unito.it) and hpc@polito at the Politecnico di Torino (www.hpc.polito.it).

References

[1] M.J. Baum, L. Heepe, E. Fadeeva, S.N. Gorb, Dry friction of microstructured polymer surfaces inspired by snake skin, Beilstein J. Nanotechnol. 5 (2014) 1091–1103, https://doi.org/10.3762/bjnano.5.122.
[2] C. Greiner, M. Schäfer, U. Popp, P. Gumbsch, Contact splitting and the effect of dimple depth on static friction of textured surfaces, ACS Appl. Mater. Interfaces 6 (2014) 7986–7990, https://doi.org/10.1021/am500879m.
[3] B. He, W. Chen, Q. Jane Wang, Surface texture effect on friction of a microtextured poly(dimethylsiloxane) (PDMS), Tribol. Lett. 31 (2008) 187–197, https://doi.org/10.1007/s11249-008-9351-0.
[4] N. Li, E. Xu, Z. Liu, X. Wang, L. Liu, Tuning apparent friction coefficient by controlled patterning bulk metallic glasses surfaces, Sci. Rep. 6 (2016) 1–9, https://doi.org/10.1038/srep39388.
[5] S. Maegawa, F. Itoigawa, T. Nakamura, Effect of surface grooves on kinetic friction of a rubber slider, Tribol. Int. 102 (2016) 326–332, https://doi.org/10.1016/j.triboint.2016.05.019.
[6] B. Murarash, Y. Itovich, M. Varenberg, Tuning elastomer friction by hexagonal surface patterning, Soft Matter 7 (2011) 5553, https://doi.org/10.1039/c1sm00015b.
[7] H.T. Tramsen, S.N. Gorb, H. Zhang, P. Manoonpong, Z. Dai, L. Heepe, Inversion of friction anisotropy in a bio-inspired asymmetrically structured surface, J. R. Soc. Interface 15 (2018) 0629, https://doi.org/10.1098/rsif.2017.0629.
[8] S. Ghio, G. Paternoster, R. Bartali, P. Belluti, M. Boscardin, N.M. Pugno, Fast and large area fabrication of hierarchical bioinspired superhydrophobic silicon surfaces, J. Eur. Ceram. Soc. 36 (2015) 2363–2369, https://doi.org/10.1016/j.jeurceramsoc.2016.01.041.
[9] S.M. Hsu, Y. Jing, D. Hua, H. Zhang, Friction reduction using discrete surface textures: principle and design, J. Phys. D. Appl. Phys. 47 (2014), 335307. https://doi.org/10.1088/0022-3727/47/33/335307.
[10] Y.C. Jung, B. Bhushan, Contact angle, adhesion and friction properties of micro-and nanopatterned polymers for superhydrophobicity, Nanotechnology 17 (2006) 4970–4980, https://doi.org/10.1088/0957-4484/17/19/033.
[11] U. Pettersson, S. Jacobson, Friction and wear properties of micro textured DLC coated surfaces in boundary lubricated sliding, Tribol. Lett. 17 (2004) 553–559, https://doi.org/10.1023/B:TRIL.0000044504.76164.4e.
[12] Z. Yoshimitsu, A. Nakajima, T. Watanabe, K. Hashimoto, Effects of surface structure on the hydrophobicity and sliding behavior of water droplets, Langmuir 18 (2002) 5818–5822, https://doi.org/10.1021/la020088p.
[13] L. Zhai, M.C. Berg, F.Ç. Cebeci, Y. Kim, J.M. Milwid, M.F. Rubner, R.E. Cohen, Patterned superhydrophobic surfaces: toward a synthetic mimic of the Namib Desert beetle, Nano Lett. 6 (2006) 1213–1217, https://doi.org/10.1021/nl060644q.
[14] L. Brely, F. Bosia, N.M. Pugno, The influence of substrate roughness, patterning, curvature, and compliance in peeling problems, Bioinspir. Biomim. 14 (2018) 5509, https://doi.org/10.1088/1748-3190/aaa0e5.
[15] H. Zeng, N. Pesika, Y. Tian, B. Zhao, Y. Chen, M. Tirrell, K.L. Turner, J.N. Israelachvili, Frictional adhesion of patterned surfaces and implications for gecko and biomimetic systems, Langmuir 25 (2009) 7486–7495, https://doi.org/10.1021/La900877h.
[16] M. Urbakh, J. Klafter, D. Gourdon, J.N. Israelachvili, The nonlinear nature of friction, Nature 430 (6999) (2004) 525–528, https://doi.org/10.1038/nature02750.
[17] B.N.J. Persson, Sliding Friction: Physical Principles and Applications, 2nd ed. Springer Berlin Heidelberg, Berlin, Heidelberg, 2000 https://doi.org/10.1007/978-3-662-04283-0.
[18] M. Nosonovsky, B. Bhushan, Multiscale friction mechanisms and hierarchical surfaces in nano- and bio-tribology, Mater. Sci. Eng. R. Rep. 58 (2007) 162–193, https://doi.org/10.1016/j.mser.2007.09.001.
[19] A. Vakis, V.A. Yastrebov, J. Scheibert, L. Nicola, D. Dini, C. Minfray, A. Almqvist, M. Paggi, S. Lee, G. Limbert, J.F. Molinari, G. Anciaux, S. Echeverri Restrepo, A. Papangelo, A. Cammarata, P. Nicolini, R. Aghababaei, C. Putignano, S. Stupkiewicz, J. Lengiewicz, G. Costagliola, F. Bosia, R. Guarino, N.M. Pugno, G. Carbone, M.H. Müser, M. Ciavarella, Modeling and simulation in tribology across scales: an overview, Tribol. Int. 125 (2018) 169–199. doi.org/https://doi.org/10.1016/j.triboint.2018.02.005.
[20] A. Filippov, S.N. Gorb, Frictional-anisotropy-based systems in biology: structural diversity and numerical model, Sci. Rep. 3 (2013) 1–6, https://doi.org/10.1038/srep01240.
[21] D.T. Nguyen, S. Ramakrishna, C. Fretigny, N.D. Spencer, Y. Le Chenadec, A. Chateauminois, Friction of rubber with surfaces patterned with rigid spherical asperities, Tribol. Lett. 49 (2013) 135–144, https://doi.org/10.1007/s11249-012-0052-3.
[22] A. Vanossi, N. Manini, M. Urbakh, S. Zapperi, E. Tosatti, Colloquium: modeling friction: from nanoscale to mesoscale, Rev. Mod. Phys. 85 (2013) 529–552, https://doi.org/10.1103/RevModPhys.85.529.
[23] U. Dehlinger, Zur Theorie der Rekristallisation reiner Metalle, Ann. Phys. 394 (1929) 749–793, https://doi.org/10.1002/andp.19293940702.
[24] T. Kontorova, J. Frenkel, On the theory of plastic deformation and twinning, I., Zhurnal Eksp. I Teor. Fiz. 8 (1938) 89–95.
[25] O.M. Braun, Y.S. Kivshar, The Frenkel-Kontorova Model: Concepts, Methods, and Applications, Springer-Verlag, Berlin, 2004 https://doi.org/10.1007/978-3-662-10331-9.
[26] M. Peyrard, S. Aubry, Critical behaviour at the transition by breaking of analyticity in the discrete Frenkel-Kontorova model, J. Phys. C Solid State Phys. 16 (1983) 1593–1608, https://doi.org/10.1088/0022-3719/16/9/005.
[27] M. Hirano, K. Shinjo, Atomistic locking and friction, Phys. Rev. B 14 (1990) 11837–11851, https://doi.org/10.1103/PhysRevB.41.11837.
[28] P.E. Sheehan, C.M. Lieber, Nanotribology and nanofabrication of MoO3 structures by atomic force microscopy, Science 272 (1996) 1158–1161, https://doi.org/10.1126/science.272.5265.1158.
[29] M. Dienwiebel, G.S. Verhoeven, N. Pradeep, J.W.M. Frenken, J.A. Heimberg, H.W. Zandbergen, Superlubricity of graphite, Phys. Rev. Lett. 92 (2004), 126101. https://doi.org/10.1103/PhysRevLett.92.126101.
[30] D. Mandelli, A. Vanossi, M. Invernizzi, S. Paronuzzi, N. Manini, E. Tosatti, Superlubric-pinned transition in sliding incommensurate colloidal monolayers, Phys. Rev. B: Condens. Matter Mater. Phys. 92 (2015) 134306, https://doi.org/10.1103/PhysRevB.92.134306.
[31] J. Norell, A. Fasolino, A.S. De Wijn, Emergent friction in two-dimensional Frenkel-Kontorova models, Phys. Rev. E 94 (2016), 023001. https://doi.org/10.1103/PhysRevE.94.023001.
[32] R. Burridge, L. Knopoff, Model and theoretical seismicity, Bull. Seismol. Soc. Am. 57 (1967) 341–371.
[33] O.M. Braun, I. Barel, M. Urbakh, Dynamics of transition from static to kinetic friction, Phys. Rev. Lett. 103 (2009) 4301, https://doi.org/10.1103/PhysRevLett.103.194301.
[34] J. Trømborg, J. Scheibert, D.S. Amundsen, K. Thøgersen, A. Malthe-Sørenssen, Transition from static to kinetic friction: insights from a 2D model, Phys. Rev. Lett. 107 (2011) 4301, https://doi.org/10.1103/PhysRevLett.107.074301.
[35] G. Costagliola, F. Bosia, N.M. Pugno, Static and dynamic friction of hierarchical surfaces, Phys. Rev. E 94 (2016) 1–10, https://doi.org/10.1103/PhysRevE.94.063003.
[36] G. Costagliola, F. Bosia, N.M. Pugno, A 2-D model for friction of complex anisotropic surfaces, J. Mech. Phys. Solids 112 (2018) 50–65, https://doi.org/10.1016/j.jmps.2017.11.015.

[37] A. Erdemir, Review of engineered tribological interfaces for improved boundary lubrication, Tribol. Int. 38 (2005) 249–256, https://doi.org/10.1016/j.triboint.2004.08.008.
[38] I. Etsion, Improving tribological performance of mechanical components by laser surface texturing, Tribol. Lett. 17 (2004) 733–737, https://doi.org/10.1007/s11249-004-8081-1.
[39] R. Ranjan, D.N. Lambeth, M. Tromel, P. Goglia, Y. Li, Laser texturing for low-flying-height media, J. Appl. Phys. 69 (1991) 5745–5747, https://doi.org/10.1063/1.347908.
[40] C.J. Rand, A.J. Crosby, Friction of soft elastomeric wrinkled surfaces, J. Appl. Phys. 106 (2009) 49131–49134, https://doi.org/10.1063/1.3226074.
[41] J. Yu, S. Chary, S. Das, J. Tamelier, K.L. Turner, J.N. Israelachvili, Friction and adhesion of gecko-inspired PDMS flaps on rough surfaces, Langmuir 28 (2012) 11527–11534, https://doi.org/10.1021/la301783q.
[42] S. Bistac, A. Galliano, Nano and macro tribology of elastomers, Tribol. Lett. 18 (2005) 21–25, https://doi.org/10.1007/s11249-004-1701-y.
[43] A. Galliano, S. Bistac, J. Schultz, Adhesion and friction of PDMS networks: molecular weight effects, J. Colloid Interface Sci. 265 (2003) 372–379, https://doi.org/10.1016/S0021-9797(03)00458-2.
[44] R. Sahli, G. Pallares, C. Ducottet, I.E. Ben Ali, S. Al Akhrass, M. Guibert, J. Scheibert, Evolution of real contact area under shear and the value of static friction of soft materials, Proc. Natl. Acad. Sci. (2018), 201706434. https://doi.org/10.1073/pnas.1706434115.
[45] G. Carbone, B. Lorenz, B.N.J. Persson, A. Wohlers, Contact mechanics and rubber friction for randomly rough surfaces with anisotropic statistical properties, Eur. Phys. J. E 29 (2009) 275–284, https://doi.org/10.1140/epje/i2009-10484-8.
[46] Y.S. Yu, Y.P. Zhao, Deformation of PDMS membrane and microcantilever by a water droplet: comparison between Mooney-Rivlin and linear elastic constitutive models, J. Colloid Interface Sci. 332 (2009) 467–476, https://doi.org/10.1016/j.jcis.2008.12.054.
[47] A. Vernes, S. Eder, G. Vorlaufer, G. Betz, On the three-term kinetic friction law in nanotribological systems, Faraday Discuss. 156 (2012) 173–196, https://doi.org/10.1039/c2fd00120a.
[48] S.J. Eder, G. Feldbauer, D. Bianchi, U. Cihak-Bayr, G. Betz, A. Vernes, Applicability of macroscopic wear and friction laws on the atomic length scale, Phys. Rev. Lett. 115 (2) (2015)https://doi.org/10.1103/PhysRevLett.115.025502.